



Sibel Oğuzlar

Merve Zeyrek Ongun

Dokuz Eylül University, İzmir-Turkey
sibel.oguzlar@deu.edu.tr; merve.zeyrek@deu.edu.tr

DOI	http://dx.doi.org/10.12739/NWSA.2019.14.4.1A0442	
ORCID ID	0000-0001-9903-7484	0000-0002-2874-8024
CORRESPONDING AUTHOR	Sibel Oğuzlar	

ENHANCEMENT OF OPTICAL OXYGEN SENSING PROPERTIES OF [Ru(BPY)₃]²⁺- BASED COMPOSITES ALONG WITH MAGHEMITE AND IONIC LIQUID

ABSTRACT

In this study, we measured oxygen-induced emission and decay-time data of tris(2,2'-bipyridyl)ruthenium(II) chloride dye in the presence of additives, maghemite and ionic liquid, 1-butyl-3-methylimidazolium tetrafluoroborate. The fluorescent dye along with the additives was embedded in ethylcellulose matrix that was used as supporting material in form of thin-film and electrospun mat. The synthesized maghemite was used to enhance the oxygen sensitivity and linear working range of the dye. Ionic liquid (IL) was used to increase the stability and sensitivity of the sensing fluorophore. Together with the additives ruthenium dye-based composites exhibited higher Stern-Volmer constant (K_{SV}), relative signal change and larger linear response. High relative signal change and KSV values mean that fluorophore has a better oxygen gas sensitivity. Stern-Volmer values of thin-film and microporous mats were found 1.64×10^{-2} and 2.21×10^{-2} , the relative signal changes (I_0/I) were calculated as 2.64 and 3.21, respectively. There is no previous work about the utilization of both maghemite and ionic liquid additives together for the enhancement of oxygen sensitivity of the ruthenium.

Keywords: Ruthenium Complex, Oxygen Sensor, Ionic Liquid, Maghemite, Fluorescence

1. INTRODUCTION

The continuous and accurate detection of dissolved and gaseous O₂ levels are of great importance in environmental [1], chemical [2], biochemical [3] and clinical analysis [4]. Nowadays optical sensors based on the spectroscopic changes [5 and 7] and electrochemical sensing approaches [8 and 9] have been used for oxygen detections. However, when compared with the electrochemical detection approaches, the optical chemical sensing techniques have some advantages like sensitivity and stability, shorter response time and low cost. There are different types of organic dyes such as transition metal complexes of osmium [10], palladium [11], iridium [12] and ruthenium [13], pyrene [14], phenanthrene [15] and metalloporphyrins [16] used as oxygen-induced optical sensors based on the working principle of quenching. Among them, the ruthenium and derivatives have been the most sensitive dye. Also, the sensing characteristics of fluorescent dyes depend on the interactions of micro-environment of dyes and the kind of polymeric material. Most of the oxygen sensing ruthenium derivatives were embedded in a gas permeable sol-gel or polymeric matrices. The appropriate polymer matrix can play a role as an enhancer agent in the oxygen sensitivity properties and provide mechanical stability due to being a rigid support material. Last

How to Cite:

Oğuzlar, S. and Zeyrek Ongun, M., (2019). Enhancement of Optical Oxygen Sensing Properties of [Ru(bpy)₃]²⁺- Based Composites Along with Maghemite and Ionic Liquid, Engineering Sciences (NWSAENS), 14(4):207-217, DOI: 10.12739/NWSA.2019.14.4.1A0442.



decades, researchers work about the enhancement of the O₂ sensitivity of ruthenium derivative dyes by supplementing some additives such as metal oxides [17], Ionic liquids [18], AgNPs [19] and AuNPs [20].

Jiang and et al. reported a ratiometric optical sensor using with tris (4,7-diphenyl-1,10-phenanthroline) ruthenium(II) dichloride (Ru(DPP)₃Cl₂) dye embedded in polymeric solid matrix in the presence of silver nano-particles as additive materials. They found an enhancement of K_{sv} values and linear working range by adding AgNPs [19]. For the detection of oxygen, the fluorescent tris (2,2'-bipyridyl) ruthenium(II) chloride [Ru(bpy)₃]²⁺ dye embedded in polymeric electrospun mats together with hydrophilic and hydrophobic ionic liquids were used and the offered composites provided higher sensitivity for oxygen and extraordinary long term stability [18]. The oxygen-induced response of the Ru(bipy)₃2 utilization of AgNPs and ILs resulted in many advantages such as increment in oxygen sensitivity and all sensor dynamics, linear calibration plot for larger concentration ranges [21]. Recently, utilizing some of the metal oxides as an additive improve the performance of gas sensors, such as stability, sensitivity, linear working range, the limit of detection and quantification. Iron oxides, which are everywhere in nature and constitute an important class of materials, are present as 16 different iron oxides/hydroxide polymorphs. Due to the variety of physical properties they have, these iron oxides are of great interest by offering application in many fields such as medicine, optoelectronics, environment and gas measurement. The most common ones are hematite (α-Fe₂O₃), maghemite (γ-Fe₂O₃) and magnetite (Fe₃O₄) [14]. The combination of small Au particles with different metal oxide structures was explained that led to measure the sensitivities of different gases via different mechanisms [22]. The intensity signal change of the ZnO₂ films was used as a transduction mechanism to recognize the presence of nitrogen oxide gas [23].

The adsorption and gas-sensing characteristics of the CO₂ and CO molecules on α-Fe₂O₃ nano-thin film matrix were investigated in the presence and absence of pre-adsorbed oxygen molecules using the density functional theory (DFT) method [24]. Additionally, the performance of α-Fe₂O₃ nanoparticles in the detection of flammable and toxic gases was investigated [25]. As described above, the ferric-oxide gas sensors measured the change of electrical conductivity in the presence of a target gas. But in this study, we investigate the emission-based oxygen sensitivity of the tris (2,2'-bipyridyl) ruthenium (II) chloride (Ru(bipy)₃²⁺) dye in the presence of ferric oxide nanoparticles, which have the oxygen adsorption ability on the surface. Herein, maghemite crystals were synthesized by chemical coprecipitation method and characterized by X-ray diffraction (XRD), scanning electron microscopy (SEM) and X-ray photoelectron spectroscopy (XPS). As far as we know, this is the first time maghemite crystals have been used as an additive that enhances the oxygen sensing properties of the [Ru(bipy)₃]²⁺ fluorophore in the EC-matrix. Effects of the metal oxide particles on oxygen sensing were measured and interpreted by steady-state and decay time-based measurements in terms of sensitivity and sensor characteristics. The maghemite particles incorporated with the fluorescent dye, embedded in the thin film and microporous mat, exhibited 62.0 and 69.0 % relative signal intensity change when exposed to the O₂, respectively.

2. RESEARCH SIGNIFICANCE

To the best of our knowledge, there is no previous work about the utilization of both maghemite and ionic liquid additives together



for the enhancement of oxygen sensitivity of the ruthenium dye. With this point of view, this research is unique in the studied field.

3. EXPERIMENTAL METHOD AND MATERIAL

3.1. Reagents

All of the chemicals used were analytical grade. Tetrahydrofuran (THF), ethanol (EtOH) and ionic liquid (IL), 1-butyl-3-methylimidazolium tetrafluoroborate, ([BMIM][BF₄]) were supplied from Merck. The oxygen-sensitive fluorescent dye, tris(2,2-bipyridyl)ruthenium(II) chloride [Ru(bpy)₃]²⁺ and the polymer membrane ethyl cellulose (with an ethoxy content of 46%) (EC), Glacial acetic acid (≥99.7 vol.%), perfluoro-compound (PFC), nonadecafluorodecanoic acid, Iron(III)-chloride-hexahydrate (FeCl₃.6H₂O), Iron(II)-chloride-tetrahydrate (FeCl₂.4H₂O), hydrochloric acid (HCl), sodium hydroxide (NaOH), nitric acid (HNO₃) were supplied from Sigma Aldrich. The plasticizer, dioctyl phthalate (DOP) was purchased from Fluka. O₂ and N₂ gas cylinders were obtained from Tinsa Gas, Izmir, Turkey.

3.2. Instrumentation

XRD analysis were carried out through Thermo Scientific ARL X-ray diffractometer. X-Ray photoelectron spectroscopy was carried out to determine elemental composition of iron oxide samples through Thermo Scientific K-Alpha. SEM images were captured at different magnification by using a JEOL JSM 6060. For the preparation of the microporous mats, a syringe pump (Top-5300) and a high voltage power supply (Gamma High Voltage ES30) were used. The fluorescence and decay time-based measurements of microporous mats and thin films were measured using Edinburgh FLSP 920 spectrometer. The emission and the decay time data were performed with a xenon lamp at the wavelength of 468 nm. The obtained χ^2 values were less than 1.5. For the gas phase studies, gas blender system (Sonimix 7000A gas blender) was used to prepare the desired oxygen concentrations between 0-100%.

3.3. Synthesis of γ -Fe₂O₃ Particles

In this study, the maghemite (γ -Fe₂O₃) powder was synthesized by chemical co-precipitation method [26]. FeCl₃ and FeCl₂ were dissolved in 0.14 M HCl by mixing in for 2-3 minutes at laboratory conditions. Under the stirring condition, 1.5 M NaOH solution was added dropwise till to obtain a black precipitate of Fe₃O₄. The obtained Fe₃O₄ particles were washed several times with ultrapure water and then 0.01 M HCl added. The obtained colloids were collected by the magnet and washed again with deionized water. Synthesized Fe₃O₄ crystals were stirred in 0.01 M HNO₃ at 90-100°C during 1 hour to obtain γ -Fe₂O₃ particles. In this way, the particles are completely oxidized to γ -Fe₂O₃.

3.4. Thin Film and Microporous Mat Preparation

Oxygen sensing thin film and microporous mat matrices were prepared by using the same materials. The EC based solid composites were produced by mixing of 240mg of EC, 192mg of plasticizer (DOP), 48mg of [BMIM][BF₄], 10mg of [Ru(bpy)₃]²⁺ dye, 10mg of PFC, 10mg of γ -Fe₂O₃ polymorph and 10ml of THF/EtOH (1:1). The polymeric cocktails were spread onto a 125mm polyester support (MylarTM type) in order to obtain the sensing thin films. The film thicknesses of the sensing slides were tested with Tencor Alpha Step 500 prophyloimeter and found to be 4.98±0.053 μ m (n=20). While the acquiring of microporous mats by electrospinning technique, the homogeneous polymeric solutions were poured into a 10 mL plastic syringe fitted with a metallic needle. The stationary voltage (25kV) between the needle and grounded aluminum

plate was applied with the high voltage supply. The polymer cocktail was feed as a rate of 2.0mL/h in laboratory conditions at 20.0°C.

4. RESULTS AND DISCUSSIONS

4.1. Characterization Studies

- XRD Analysis:** XRD pattern of γ -Fe₂O₃ particles is shown in Figure 1a. The XRD pattern reveals all of the major peaks of γ -Fe₂O₃ particles, corresponding to the spinel cubic structure and the value of lattice parameter is in agreement with the values of the standard data (JCPDS no. 39-1346). The related diffraction peaks of γ -Fe₂O₃ particles at (220), (311), (400), (422), (511) and (440) are identified in the XRD patterns as similarly with the literature [27].
- Elemental Analysis:** XPS measurements were performed to determine the surface chemical composition of maghemite particules which include related elements, binding energies (B.E), and weight concentration (wt. %). The results are summarized in Table 1. The binding energy peaks around 711 eV for the Fe2p, 530 eV for the O1s, and 285 eV for the C1s (Figure 1b) were in evidence for γ -Fe₂O₃ were shown in Figure 1b. The observed C1s peak for sample is expected to be derived from the fortuitous hydro-carbon from the external contaminants or XPS instrument itself which are in agreement with the peak positions and values that reported in the literature [28].
- Particle Morphology:** The surface morphology and microstructure of the porous γ -Fe₂O₃ particles were characterized by SEM. The SEM images of maghemite powders are shown in Figure 1c. It can be seen from the SEM image of powders that the particles are agglomerated. The size distribution and morphology are irregular.

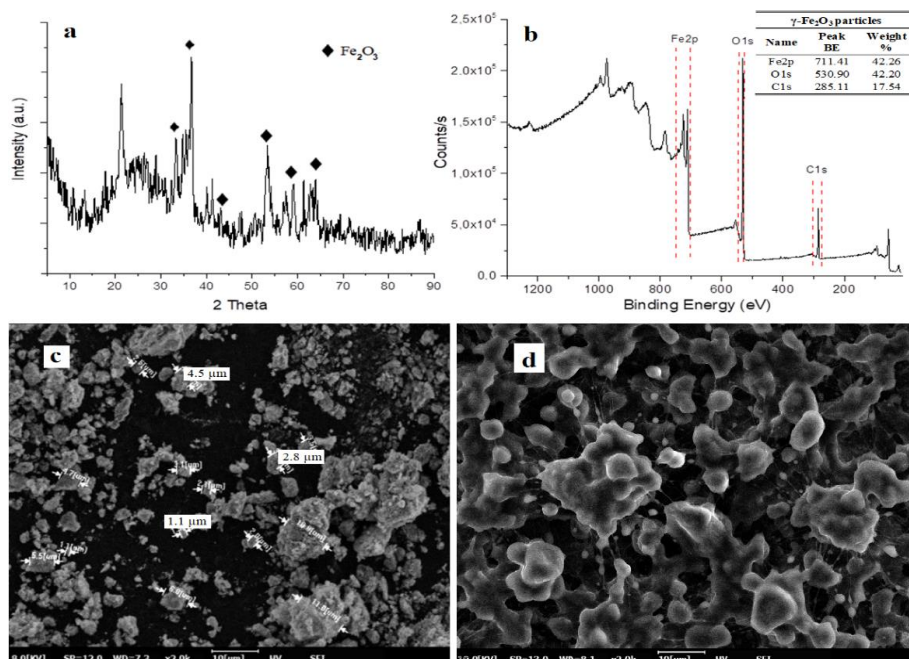


Figure 1. The characterization of γ -Fe₂O₃ crystals by means of structural and morphological properties by using, a:XRD, b:XPS. SEM images of c: γ -Fe₂O₃ particles and d:the γ -Fe₂O₃-doped [Ru(bpy)₃]²⁺ dye in EC electrospun mat at $\times 2000$ magnification



4.2. Effect of Additives on Oxygen Sensing Ability of the $[\text{Ru}(\text{bpy})_3]^{2+}$

Long et al., reported the gas-sensing mechanisms of ferric oxide are generally based on the direct chemisorption or a surface state associated with the adsorbed oxygen on the surface of p- or n-type metal oxide. Also, they explained that the gas sensing properties of ferric oxide were improved as reducing the diameter and increasing their surface area [29]. In the light of the literature, we tested oxygen sensitivity of the ruthenium dye when used along with maghemite and ionic liquid expecting an enhancement in the emission performance of the dye through O_2 adsorption ability of ferric oxide. Herein, we investigated the O_2 sensitivity of the fluorescent dye along with maghemite particles in the polymeric matrix, in the form of thin-film and microporous mat. All of the studied forms include ionic liquid, $[\text{BMIM}][\text{BF}_4]$, to enhance the characteristics of oxygen diffusion of the sensing slides [18]. When all of the studied composites excited at 468 nm, the maximum emission wavelength of the ruthenium in EC based media-centered at 620 nm accompanied by the signal drops. The intensity response of the maghemite free- $[\text{Ru}(\text{bpy})_3]^{2+}$ dye was measured for the concentration range of 0-100% $p[\text{O}_2]$ (Figure 2). Figure 2b and Figure 2c reveal the oxygen-induced variations of the emission spectra of the $\gamma\text{-Fe}_2\text{O}_3$ including fluorescent dye embedded in the thin film and microporous mat form, respectively.

The additive-free $[\text{Ru}(\text{bpy})_3]^{2+}$ dye-doped microporous sensing slides exhibited at 61.0% of intensity-based signal drop, besides, the dye utilized along with maghemite in form of thin-film and microporous mat yielded 62.0 and 69.0% signal changes towards oxygen for the concentration range of 0-100%, respectively. Consequently, it can be seen from the results, when the maghemite used as an additive in microporous sensing slides became more sensitive towards oxygen than additive free-dye. All of the signal change of the sensing composites could be linearized by least squares algorithm (Figure 2d) and they yielded good R^2 values. However, the linearized calibration plots, the correlation coefficients for the concentration range of 0-100% $p[\text{O}_2]$, the K_{SV} values of the utilized composites and sensitivities (I_0/I_{100}) were shown in Table 2. The sensitivity of an oxygen-induced is represented by the ratio of I_0/I_{100} and the Stern-Volmer constant. The following K_{SV} equation (Equation 1) shows the relationship between the fluorescence decay-times and/or emission-based intensities and the concentration of the quencher:

$$I_0/I = \tau_0/\tau = 1 + K_{\text{SV}}[\text{O}_2] = 1 + k_q\tau_0[\text{O}_2] \quad (1)$$

where I_0 and I are the emission intensities under deoxygenated and fully-oxygenated conditions respectively, the K_{SV} is the Stern-Volmer constant which quantifies the efficiency of the sensor, and, $[\text{O}_2]$ is the concentration of the triplet oxygen [30].

Here in, the I_0/I_{100} values were recorded at 2.55, 2.64 and 3.21 for the additive-free $[\text{Ru}(\text{bpy})_3]^{2+}$ dye, and, in the presence of the maghemite-additive in the thin film and microporous mat, respectively. The K_{SV} values determined from slopes of the calibration plots were found to be 2.21×10^{-2} and 1.64×10^{-2} ($\%^{-1}$) for the electrospun mat and thin film of maghemite-doped ruthenium dye, respectively. From the Table 2, it can be concluded that the $\gamma\text{-Fe}_2\text{O}_3$ -doped $[\text{Ru}(\text{bpy})_3]^{2+}$ embedded in the microporous mat showed higher relative signal change and K_{SV} value, so it showed better oxygen gas sensitivity with respect to the other sensing slides.

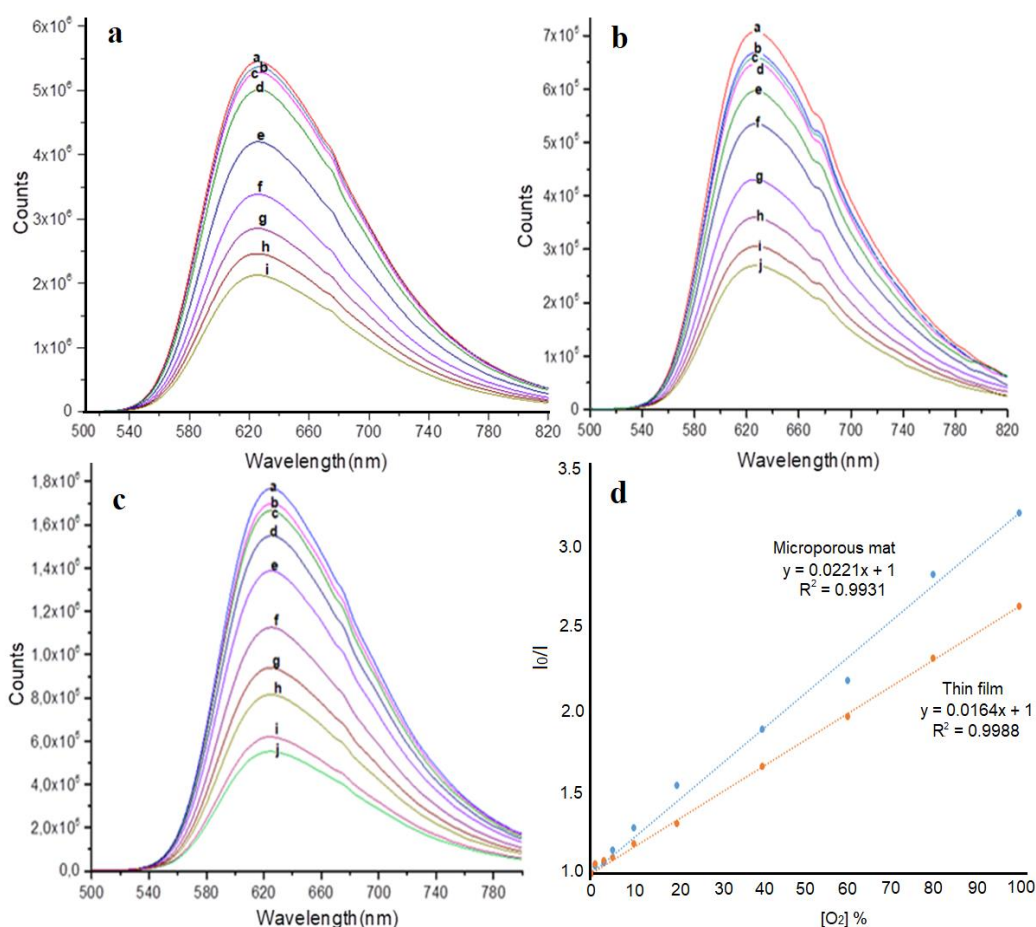


Figure 2. Intensity-based signal change of a: γ - F_2O_3 -free $[Ru(bpy)_3]^{2+}$ dye in EC electrospun mat, b: γ - F_2O_3 -doped $[Ru(bpy)_3]^{2+}$ dye in EC thin film, c: γ - F_2O_3 -doped $[Ru(bpy)_3]^{2+}$ dye in EC microporous mat upon exposure to the oxygen concentrations of a:0%, b:1%, c:3%, d:5%, e:10%, f:20%, g:40%, h:60%, i:80%, j:100%, d:Stern-Volmer plot derived from quenching based data both the γ - F_2O_3 doped EC based sensing microporous mat and thin film

The enhancement in the diffusion ability of the oxygen and consequently in the sensitivity was an expected result for us because of O_2 adsorption ability of ferric oxide particles. In order to clarify the mechanism lying behind the interaction between maghemite additive and the fluorescent dye, we recorded the emission and excitation spectra of the $[Ru(bpy)_3]^{2+}$ and γ - F_2O_3 particles separately. Table 3 reveals the absorption and emission maxima of the dye and the additives embedded in EC thin film when excited at 468nm, respectively. Maghemite powders strongly absorbed between 290-550nm and emitted at a large wavelength range between 450 and 780nm covering the excitation band of the $[Ru(bpy)_3]^{2+}$. The emission band of the γ - F_2O_3 overlaps with the excitation band of the $[Ru(bpy)_3]^{2+}$ dye when excited at the 468nm. It means there is an energy transfer between the γ - F_2O_3 particles and the ruthenium dye possible. However, there is a completely overlap between the excitation band of the γ - F_2O_3 and the excitation band of the ruthenium. These properties make the maghemite powders potential energy transmitter agents.



Table 2. Emission and excitation maxima, O₂ sensing agent (I₀/I₁₀₀), linearized calibration plots and Ksv values of the dye in EC thin films and electrospun mats when excited at 468 nm in the absence and the presence of the additives

Composite	Matrix/Polymer	Amount of ILs (mg)	Amount of γ -e ₂ O ₃ (mg)	λ_{ex} (nm)	λ_{em} (nm)	Linearized Calibration Plots	Ksv (% ⁻¹)	Reg. Coef. R ²	I ₀ /I ₁₀₀
γ -Fe ₂ O ₃	Thin Film/EC	-	-	480	560	-	-	-	-
[Ru (bpy) ₃] ²⁺	Thin Film/EC	-	-	468	620	-	-	-	-
γ -Fe ₂ O ₃ -free [Ru (bpy) ₃] ²⁺	Mat/EC	10	-	468	622	y=0.0153x+1	1.53×10 ⁻²	0.9970	2.55
γ -Fe ₂ O ₃ -doped [Ru (bpy) ₃] ²⁺	Thin Film/EC	10	10	468	622	y=0.0164x+1	1.64×10 ⁻²	0.9988	2.64
γ -Fe ₂ O ₃ -doped [Ru (bpy) ₃] ²⁺	Mat/EC	10	10	468	622	y=0.0221x+1	2.21×10 ⁻²	0.9931	3.21

4.3. Decay-time Measurements of the Sensor Slides

In order to understand the O₂ sensitivity of the [Ru(bpy)₃]²⁺ in the presence of γ -Fe₂O₃ additive, and to explain the energy transfer from maghemite to the fluorescent dye, we evaluated the oxygen-induced decay time-based data. The recorded decay times were shown in Table 3 for both thin film and the microporous mat of the γ -Fe₂O₃-doped [Ru(bpy)₃]²⁺. As seen from Table 3, the ruthenium dye exhibited multi-exponential decay in all of the employed matrices. The measured decay time levels decreased from 299.49 to 219.85 ns for thin film and from 335.41 to 183.48ns for electrospun mat under fully-oxygenated conditions, respectively. This variation in the decay time values can be attributed to the difficulties of the accessibility of the quencher. The highly porous structures of electrospun mats exhibited shorter fluorescence decay times with respect to the less porous material of thin films, because of the higher O₂ diffusion abilities of the empty spaces of the holes within the porous structures. Dynamic quenching decreases both of the decay time and the emission-based intensities of the quenched fluorophore. Therefore, the mechanism of the quenching observed here can be concluded as a dynamic type.

Table 3. Fluorescence decay times of γ -Fe₂O₃-doped [Ru(bpy)₃]²⁺ in EC matrix for thin film and microporous mat forms

Composite	Matrix	τ_0 (0% O ₂)	Decay Time (ns)	Std. Dev. (ns)	Rel. (%)	τ_0 (100% O ₂)	Decay Time (ns)	Std. Dev. (ns)	Rel. (%)
		τ_1	0.5813	0.00485	1.35	τ_1	0.6034	0.00389	3.05
γ -Fe ₂ O ₃ -doped [Ru(bpy) ₃] ²⁺	Thin Film	τ_2	5.4068	0.60171	0.25	τ_2	6.2167	0.49679	0.59
		τ_3	304.3392	19.0348	98.40	τ_3	228.1033	10.2742	96.36
		τ_{avr}		299.49ns		τ_{avr}		219.85ns	
		τ_1	0.5743	0.00417	0.77	τ_1	0.5868	0.00547	2.35
γ -Fe ₂ O ₃ -doped [Ru(bpy) ₃] ²⁺	Mat	τ_2	56.8005	2.01770	0.57	τ_2	9.5126	4.24807	0.20
		τ_3	339.6359	3.65205	98.66	τ_3	188.2486	9.48129	97.45
		τ_{avr}		335.41ns		τ_{avr}		183.48 s	

4.4. Reproducibility and Stability Performances

Reversibility, reproducibility, and stability performances were investigated for the [Ru(bpy)₃]²⁺ dye-doped electrospun mat in the presence of the maghemite additive. The emission-based kinetic response and reversibility performance test of the oxygen-induced sensing slide was performed on going from 100% O₂ to 100% N₂. The response time which is the time taken to attain 80% of the signal intensity when the gas is changed, was found to be 50s. The regeneration time of the microporous mat was measured 70s when going from fully-oxygenated to the de-oxygenated atmosphere. After exposure to oxygen concentration at the range of 0-100% by twenty-six replicate measurements, the standard deviation of upper and lower signal levels were found to be 45.33×10²±90.1 and 16.37×10²±30.4 (n=26), respectively. We have indicated that the [BMIM⁺][BF₄⁻] doped sensor agents exhibited a stable and reproducible response for oxygen measurements.

5. CONCLUSION

In this study, we investigated O₂ induced sensitivity of the [Ru(bpy)₃]²⁺ dye in the presence of γ -Fe₂O₃ by fluorescence and decay time measurements in the EC polymeric matrix. The synthesized maghemite particles were characterized by XRD, XPS, and SEM. We prepared the O₂ sensitive materials in the form of both thin films and microporous mats. In a form of electrospun mats, we observed enhanced sensitivity for the oxygen with respect to the thin film. The intensity-based oxygen response of the fluorescent dye in the presence of the additives, γ -Fe₂O₃ and [BMIM⁺][BF₄⁻], exhibited higher oxygen sensitivity and K_{SV} constant, better relative signal changes and more linear calibration plots under the concentration range of 0-100% [O₂] when compared with the additive-free [Ru(bpy)₃]²⁺.



ACKNOWLEDGMENTS

All authors would like to thank to Dokuz Eylul University, Center for Fabrication and Applications of Electronic Materials (EMUM) for XRD, XPS, SEM, and PL measurements.

NOTICE

This study was presented and reconstructed at the 2nd International Eurasian Biological and Chemical Sciences Conference held between 28-29 June 2019.

REFERENCES

- [1] Nault, L., Bouchab, L., Dupré-Crochet, S., Nüße, O., and Erard, M., (2016). Environmental Effects on Reactive Oxygen Species Detection—Learning from the Phagosome. *Antioxidants & redox signaling*, 25(10):564-576.
- [2] Ando, M., (2006). Recent Advances in Optochemical Sensors for the Detection of H₂, O₂, O₃, CO, CO₂ and H₂O in Air. *TrAC Trends in Analytical Chemistry*, 25(10):937-948.
- [3] Hardy, M., Zielonka, J., Karoui, H., Sikora, A., Michalski, R., Podsiadły, R., Lopez, M., Vasquez-Vivar, J., Kalyanaraman, B., and Ouari, O., (2018). Detection and Characterization of Reactive Oxygen and Nitrogen Species in Biological Systems by Monitoring Species-Specific Products. *Antioxidants & redox signaling*, 28(15):1416-1432.
- [4] McNeil, C.J., Athey, D., and Ho, W.O., (1995). Direct Electron Transfer Bioelectronic Interfaces: Application to Clinical Analysis. *Biosensors and Bioelectronics* 10(1-2):75-83.
- [5] Wang, X. and Wolfbeis, O.S., (2015). Fiber-Optic Chemical Sensors and Biosensors (2013-2015). *Analytical chemistry* 88(1):203-227.
- [6] Raj, D.R., Prasanth, S., Vineeshkumar, T.V., and Sudarsanakumar, C., (2016). Surface Plasmon Resonance Based Fiber Optic Dopamine Sensor Using Green Synthesized Silver Nanoparticles. *Sensors and Actuators B: Chemical* 224, 600-606.
- [7] Degler, D., Barz, N., Dettinger, U., Peisert, H., Chasse, T., Weimar, U., and Barsan, N., (2016). Extending the Toolbox for Gas Sensor Research: Operando UV/Vis Diffuse Reflectance Spectroscopy on SnO₂-Based Gas Sensors. *Sensors and Actuators B: Chemical*, 224, 256-259.
- [8] Imai, K., Okazaki, T., Hata, N., Taguchi, S., Sugawara, K., and Kuramitz, H., (2015). Simultaneous Multiselective Spectroelectrochemical Fiber-Optic Sensor: Demonstration of the Concept Using Methylene Blue and Ferrocyanide. *Analytical chemistry*, 87(4):2375-2382.
- [9] Yuan, Y., Guo, T., Qiu, X., Tang, J., Huang, Y., Zhuang, L., Zhou, S., Li, Z., Guan, B.O., and Zhang, X., (2016). Electrochemical Surface Plasmon Resonance Fiber-Optic Sensor: In Situ Detection of Electroactive Biofilms. *Analytical chemistry* 88(15):7609-7616.
- [10] Borisov, S.M., Alemayehu, A., and Ghosh, A., (2016). Osmium-Nitrido Corroles as NIR Indicators for Oxygen Sensors and Triplet Sensitizers for Organic Upconversion and Singlet Oxygen Generation. *Journal of Materials Chemistry C*, 4(24):5822-5828.
- [11] Liu, L., Wang, X., Hussain, F., Zeng, C., Wang, B., Li, Z., Kozin, I., and Wang, S., (2019). Multiresponsive Tetradentate Phosphorescent Metal Complexes as Highly Sensitive and Robust Luminescent Oxygen Sensors: Pd (II) Versus Pt (II) and 1, 2, 3-Triazolyl Versus 1, 2, 4-Triazolyl. *ACS applied materials & interfaces*, 11(13):12666-12674.



- [12] Medina-Rodríguez, S., Denisov, S.A., Cudré, Y., Male, L., Marín-Suárez, M., Fernández-Gutiérrez, A., Fernández-Sánchez, J.F., Tron, A., Jonusauskas, G., and McClenaghan, N.D., (2016). High Performance Optical Oxygen Sensors Based on Iridium Complexes Exhibiting Interchromophore Energy Shuttling. *Analyst*, 141(10):3090-3097.
- [13] Ongun, M.Z., Oter, O., Sabancı, G., Ertekin, K., and Çelik, E., (2013). Enhanced Stability of Ruthenium Complex in Ionic Liquid Doped Electrospun Fibers. *Sensors and Actuators B: Chemical* 183, 11-19.
- [14] Ye, J.W., Zhou, H.L., Liu, S.Y., Cheng, X.N., Lin, R.B., Qi, X.L., Zhang, J.P., and Chen, X.M., (2015). Encapsulating Pyrene in a Metal-Organic Zeolite for Optical Sensing of Molecular Oxygen. *Chemistry of Materials* 27(24):8255-8260.
- [15] Hurtubise, R.J., Ackerman, A.H., and Smith, B.W., (2001). Mechanistic Aspects of the Oxygen Quenching of the Solid-Matrix Phosphorescence of Perdeuterated Phenanthrene on Partially Hydrophobic Paper. *Applied Spectroscopy*, 55(4):490-495.
- [16] Topal, S.Z., Ongun, M.Z., Önal, E., Ertekin, K., and Hirel, C., (2017). Hyperporphyrin Effect on Oxygen Sensitivity of Free Meso-Tetraphenylporphyrins. *Dyes and Pigments* 144, 102-109.
- [17] Hosseini, M., Pur, M.R.K., Norouzi, P., Moghaddam, M.R., and Ganjali, M.R., (2017). An Enhanced Electrochemiluminescence Sensor Modified with a Ru (Bpy) $32^{+}/\text{Yb}_2\text{O}_3$ Nanoparticle/Nafion Composite for the Analysis of Methadone Samples. *Materials Science and Engineering: C*, 76, 483-489.
- [18] Ongun, M.Z., Oter, O., Sabancı, G., Ertekin, K., and Celik, E., (2013). Enhanced Stability of Ruthenium Complex in Ionic Liquid Doped Electrospun Fibers. *Sensors and Actuators, B: Chemical* 183, 11-19. <https://doi.org/10.1016/j.snb.2013.03.060>.
- [19] Jiang, Z., Yu, X., Zhai, S., and Hao, Y., (2017). Ratiometric Dissolved Oxygen Sensors Based on Ruthenium Complex Doped with Silver Nanoparticles. *Sensors*, 17(3):548-553.
- [20] Roche, P.J.R., Cheung, M.C.K., Yung, K.Y., Kirk, A.G., Chodavarpu, V.P., and Bright, F.V., (2010). Application of Gold Quenching of Luminescence to Improve Oxygen Sensing Using a Ruthenium (4, 7-Diphenyl-1, 10-Phenanthroline) 3Cl_2 : TEOS Thin Film. *Sensors and Actuators B: Chemical*, 147(2):581-586.
- [21] Ozturk, O., Oter, O., Yildirim, S., Subasi, E., Ertekin, K., Celik, E., and Temel, H., (2014). Tuning Oxygen Sensitivity of Ruthenium Complex Exploiting Silver Nanoparticles. *Journal of Luminescence*, 155, 191-197.
- [22] Ando, M., Kobayashi, T., and Haruta, M., (1997). Combined Effects of Small Gold Particles on the Optical Gas Sensing by Transition Metal Oxide Films. *Catalysis Today*, 36(1):135-141.
- [23] Valerini, D., Cretì, A., Caricato, A.P., Lomascolo, M., Rella, R., and Martino, M., (2010). Optical Gas Sensing through Nanostructured ZnO Films with Different Morphologies. *Sensors and Actuators B: Chemical*, 145(1):167-173.
- [24] Shi, C., Chen, Y., Liu, H., Cui, G., Ju, L., and Chen, L., (2016). Adsorption and Gas-Sensing Characteristics of a Stoichiometric $\alpha\text{-Fe}_2\text{O}_3$ (001) Nano Thin Film for Carbon Dioxide and Carbon Monoxide with and without Pre-Adsorbed O_2 . *RSC Advances* 6(5):3514-3525.
- [25] Cuong, N.D., Hoa, T.T., Khieu, D.Q., Hoa, N.D., and Van Hieu, N., (2012). Gas Sensor Based on Nanoporous Hematite Nanoparticles: Effect of Synthesis Pathways on Morphology and Gas Sensing Properties. *Current Applied Physics* 12(5):1355-1360.



-
- [26] Lin, Y., Xu, G., Wei, F., Zhang, A., Yang, J., and Hu, Q. (2016). Detection of CEA in Human Serum Using Surface-Enhanced Raman Spectroscopy Coupled with Antibody-Modified Au and γ -Fe₂O₃@ Au Nanoparticles. *Journal of Pharmaceutical and Biomedical Analysis*, 121, 135-140.
- [27] Singh, B.P., Kumar, A., Areizaga-Martinez, H.I., Vega-Olivencia, C.A., and Tomar, M.S., (2017). Synthesis, Characterization, and Electrocatalytic Ability of γ -Fe₂O₃ Nanoparticles for Sensing Acetaminophen. *Indian Journal of Pure & Applied Physics (IJPAP)*, 55(10):722-728.
- [28] Moulder, J.F., (1995). Handbook of X-Ray Photoelectron Spectroscopy. *Physical Electronics* 230-232.
- [29] Long, N.V., Teranishi, T., Yang, Y., Thi, C.M., Cao, Y., Nogami, M., (2015). Iron Oxide Nanoparticles for next Generation Gas Sensors. *International Journal of Metallurgical & Materials Engineering* 2015.
- [30] Lakowicz, J.R., (2006). Principles of Fluorescence Spectroscopy, 2006. Springer Science+ Business Media, LLC.